Assessing the Role of Interfacial Electrostatics in Oriented Mineral Nucleation at Charged Organic Monolayers

Michael J. Lochhead, Shelli R. Letellier, and Viola Vogel*

Department of Bioengineering, University of Washington, Seattle, Washington 98195

Received: July 14, 1997; In Final Form: October 11, 1997[⊗]

Charged organic−aqueous interface electrostatics are assessed in order to clarify potential electrostatic contributions to oriented mineral nucleation at planar organic surfaces. Fatty acid and acidic phospholipid monolayers contacting aqueous solutions of sparingly soluble salts serve as model systems. Monolayer electrostatic parameters and ion distributions in the interfacial aqueous solution are calculated using a Gouy−Chapman−Stern electric double-layer model that incorporates the multiple, multivalent cations and anions found in mineralizing solutions. The calculations provide insight into the relationship between surface-directed crystallization and factors such as ion binding, surface charge density, and interfacial ion concentrations. Variations in crystal nucleation, phase, and morphology observed at charged monolayers are interpreted in terms of calculated departures from lattice ion stoichiometry and pH lowering within the interfacial aqueous solution. Lattice matching is addressed in terms of Stern layer calculations of Ca^{2+} ion binding at carboxylic acid monolayers. Arguments are presented suggesting that near negatively charged surfaces, soluble ionic species concentrations are enhanced relative to free anion concentrations, and a link between interfacial anion speciation and oriented mineral nucleation is proposed. Implications for biomineralization and template-directed crystallization at planar surfaces are discussed.

Introduction

Mineral formation at organic surfaces in both natural and synthetic systems is affected by physical, chemical, and molecular interactions at the organic−aqueous interface. A substantial research effort has been aimed at developing a detailed understanding of interfacial interactions associated with biomineralization[1−5] and surface- or template-directed crystallization.[6−20] The intent has been to provide insight into natural phenomena such as bone, tooth, and shell formation, as well as to assist scientists and engineers applying biomimetic strategies to the development of novel materials such as advanced composites and coatings for medical, chemical, optical, and electronic applications.[10−13] Although progress has been made, our ability to control the orientation, phase, and morphology of surface-grown crystals is still limited. Part of the difficulty lies in the fact that no single factor dominates oriented nucleation. In addition to complicated heterogeneous nucleation thermodynamics,[21] poorly understood molecular phenomena including hydrogen bonding, dipolar interactions, and molecular recognition events such as stereochemistry and geometrical lattice matching all may play some role.[7]

Electrostatic interactions at charged surfaces are a widely recognized as significant in surface-directed mineralization.[4,7,16,18−20] Biomineralization is closely linked with negatively charged macromolecules,[1,2,5] and experiments in synthetic systems have shown that negatively charged surfaces such as functionalized polymers,[10] self-assembled monolayers and thin films,[13−17] and Langmuir monolayers[6−9,19−20] can alter mineral formation. Roles cited for the negatively charged surfaces include cation binding, cation concentration enhancement, and the orientation-specific stabilization of crystal nuclei.[22] A molecular understanding of how electrostatic interactions contribute to oriented nucleation, however, is not currently available. In addition, relatively few studies have attempted to quantitatively assess factors such as surface charge density, ion binding, and interfacial ion distributions in mineralizing systems.

In this paper we investigate the functional connection between mineral nucleation at planar, charged monolayer surfaces and classical electrostatic parameters such as surface charge density, specific ion binding, and interfacial ion distributions, with the intent of providing new insights and an improved molecular understanding of electrostatic contributions to oriented mineral nucleation. A Poisson−Boltzmann-based calculations of electrostatic parameters for different mineralizing systems serves as the basis of our analysis. The model moves beyond the familiar Gouy−Chapman equations for symmetric electrolytes and incorporates the multiple, multivalent cations and anions encountered in mineralizing solutions. Chemical specificity is introduced through intrinsic binding constants and a Langmuir adsorption isotherm Stern layer approximation. Representative calculations illustrate that in addition to forming the commonly discussed bound cation layer, charged surfaces alter the interfacial solution within which nuclei form. Mineral nucleation is discussed in terms of the cation-to-anion ratio near negatively charged surfaces, and we postulate a link between anion speciation and oriented mineral nucleation. We conclude that an improved quantitative understanding of interfacial electrostatic parameters offers new insight into the relationship between experimentally observed electrostatic effects and the molecular mechanisms of oriented mineral nucleation.

Theory

Our theoretical approach is based on the Gouy−Chapman−Stern (GCS) solutions to the Poisson−Boltzmann (PB) equation for charged, planar surfaces. Details of GCS theory can be found in numerous reviews.[23−26] The theory makes several important simplifying assumptions discussed below for our model system. Readers are directed to more thorough discussions of GCS assumptions in the context of phospholipid membrane electrostatics[27] and Langmuir monolayers.[28] In

* Corresponding author. Email: vogel@bioeng.washington.edu.
[⊗] Abstract published in *Advance ACS Abstracts,* December 1, 1997.

S1089-5647(97)02283-9 CCC: $14.00

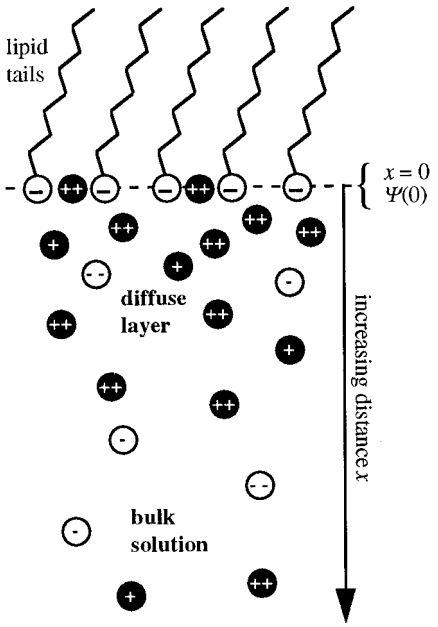

Figure 1. Schematic of the charged organic−aqueous interface region. An ordered array of negatively charged lipid molecules exists at the air−water interface. Headgroup charge is assumed smeared in the plane at $x = 0$. Counterions (in this case cations) exist in two states: bound to the negative surface and/or electrically attracted to it. Cation binding occurs at the $x = 0$ plane. $\Psi(0)$ is the Stern surface potential.

general, it has been noted that many aspects of charged lipid membrane and planar monolayer electrostatics are remarkably well-described by the relatively simple theory.[27−32] The GCS model in this section best describes planar surfaces with closely spaced surface functionalities contacting relatively dilute (<0.05 M) electrolyte solutions. These conditions are met in numerous experimental studies of sparingly soluble salts (e.g., CaC_2O_4, $CaCO_3$, $BaSO_4$, $CaSO_4$, etc.) nucleating at Langmuir monolayers[7−9,20] or self-assembled monolayers.[16]

The model system underlying our calculations is shown in Figure 1. Ordered monolayers of negatively charged lipid molecules contact an aqueous solution containing multiple electrolytes. The positively charged counterions in the interface region exist in two states. All counterions experience an electrostatic attraction and form the diffuse electric double layer. Some counterions (especially divalent counterions) also specifically bind to the surface.[28] Ion binding occurs in a Stern plane defined at $x = 0$. Ion binding serves to decrease the surface charge density σ at $x = 0$. The resultant electric potential $\Psi(0)$ is the Stern surface potential.

The GCS model used to describe this system makes the following simplifying assumptions: the surface charge is assumed to be uniformly smeared in the plane of the surface; ions are treated as point charges; and the solvent dielectric is assumed constant and equal to the pure solvent value. The smeared surface charge assumption neglects discreteness-of-charge effects in the monolayer. Although lipid monolayers are comprised of discretely charged groups, when the distance between charges is smaller than the Debye length of the aqueous subphase, a condition met in many surface-directed mineralization experiments, then discreteness-of-charge effects are minimal.[27] This was recently demonstrated in lipid bilayer and monolayer electrostatics simulations performed by Peitzsch et al.[30] For monolayers of closely packed acidic phospholipids, the simulations showed that equipotential surfaces were planar to within a few angstroms of the surface and that simple Gouy−Chapman theory predictions were accurate.[30] This is an important concept given the renewed interest in the role of uniform electric fields in surface-directed nucleation.[33] Point charges are assumed for the solutes, also as a first approximation. We restrict our analysis to relatively dilute solutions (ionic strength < 0.02 M) and note that the ions considered in our analysis are all smaller than the solution Debye length, minimizing size effects.[27] The constant solvent dielectric is a more difficult assumption to justify. Interfacial water ordering[34] and image charge effects[35] may alter ion concentrations adjacent to the surface. The effect of both the point charge and solvent dielectric assumptions could be an overestimation of interfacial ion concentrations, especially within 10 Å of the surface. Uncertainties in the calculations, however, do not compromise our interpretations. Our intent is to delineate how electrostatic parameters change as experimental conditions are varied and to relate these effects to mineral nucleation mechanisms.

Potential Profile and Ion Distributions in the Electric Double Layer. In the case of a planar interface with a uniformly smeared surface charge, the mean electric potential, Ψ, is a function only of distance normal to the interface ($\Psi = \Psi(x)$). Assuming thermal equilibrium, Boltzmann statistics are used to calculate the average ion concentrations as a function of the mean electric potential:

$$n_i(x) = n_{i,\mathrm{b}} \exp\left(\frac{-z_i e \Psi(x)}{kT}\right) \tag{1}$$

$n_i(x)$ is the number density (ions/m^3) of ion i at a distance x normal to the surface, $n_{i,\mathrm{b}}$ is the bulk concentration of ion i, z_i is the ion valence (including sign), e is the electric charge constant, $\Psi(x)$ is the mean electric potential at x in volts, k is the Boltzmann constant, and T is temperature. At 25 °C, $kT/e = 25.69$ mV.

The starting point of the theoretical treatment is the one-dimensional Poisson−Boltzmann (PB) equation:

$$\frac{\mathrm{d}^2\Psi}{\mathrm{d}x^2} = -\frac{e}{\epsilon\epsilon_0}\sum_i^m z_i n_i \exp\left(\frac{-z_i e \Psi(x)}{kT}\right) \tag{2}$$

ϵ is the dielectric constant of the solvent ($\epsilon \approx 80$ for water), ϵ_0 is the vacuum permittivity, and m is the number of ionic species.

Exact solutions of the PB equation have been derived for the special case of a symmetric $+z{:}-z$ electrolyte and other relatively simple systems. Mineralizing solutions, however, most often contain multiple, asymmetric electrolytes, including multivalent cations and anions. Analytical $\Psi(x)$ expressions for complicated electrolyte solutions are much more difficult to derive. We therefore perform the second integration of the PB equation numerically. The integral is of the form

$$x + D = \int \frac{\mathrm{d}\Psi}{\left[\frac{2kT}{\epsilon\epsilon_0}\sum_i^m n_{i,\mathrm{b}}\left(\exp\left(\frac{-z_i e \Psi(x)}{kT}\right) - 1\right)\right]^{1/2}} \tag{3}$$

D is the integration constant determined with the known $\Psi(0)$ at $x = 0$ (calculation of $\Psi(0)$ using the Grahame equation is discussed below). The accuracy of our numerical integration algorithm was checked by reproducing the analytical potential profile derived for symmetric electrolytes. We also confirmed that the excess charge density in the double layer predicted by the numerically calculated $\Psi(x)$ matched the known surface charge density.

To assess the thickness of the double layer given by eq 3, we report the value of the first e-folding ($1/e$) of the electric

TABLE 1: Instrinsic Binding Constants, K_{int} (M^{-1})

ion	phosphatidylserine (PS) $\log_{10}(K_{int})$[a]	carboxylic acid $\log_{10}(K_{int})$
Ca^{2+}	1.48	0.51[b]
Na^+	−0.22	−0.771[b]
H^+	3.5	5.4[c]

[a] Reference 29. [b] Reference 41. [c] References 42, 43.

potential decay. For a purely exponential decay, the first *e*-folding is identical with the Debye length $1/\kappa$, where $\kappa = (e^2(\Sigma n_{i,b} z_i^2)/\epsilon\epsilon_0 kT)^{1/2}$.

Monolayer Surface Charge Density, Surface Potential, and Ion Binding. Several Poisson−Boltzmann-based models have been developed to assess ion binding to organic surfaces.[28,36−40] Our approach is based on the McLaughlin methodology,[36] extended to include H^+ binding. It is described briefly here.

Experimental pressure−area isotherms are used to determine the area per molecule in the monolayer, A_m. When monovalent acidic headgroups are fully dissociated, the surface charge density σ of the monolayer is simply $-e/A_m$. Ion binding modifies the surface charge density σ at $x = 0$ relative to the completely dissociated state. We account for ion binding by assuming that specific binding of cations to the monolayer is described by a Langmuir adsorption isotherm:

$$K_{int} = \frac{\{ML\}}{\{L\}[M]_0} \tag{4}$$

K_{int} is an intrinsic binding constant and has the units L/mol; {ML} is the surface concentration (m^{-2}) of the ion−ligand (lipid headgroup) complex; {L} is the surface concentration (m^{-2}) of available headgroup binding sites; and $[M]_0$ is the volume concentration (mol/L) of the ion of interest in the aqueous phase adjacent to the surface. It should be noted that $[M]_0$ can be significantly different from the bulk ion concentration. $[M]_0$ is related to the bulk value through the Boltzmann equation (eq 1). It is for this reason K_{int} is referred to as an "intrinsic" rather than "apparent" binding constant. Intrinsic binding constants are based on ion concentrations at the interface. Apparent binding constants are based on ion concentrations in the bulk. It should also be stressed that the 1:1 ion to lipid binding assumed in eq 4 is not intended to imply a binding mechanism; we note, for example, that our model correctly predicts the approximately 1:2 ratio expected for Ca^{2+} binding to negatively charged phospholipid headgroups.

The intrinsic binding constants K_{int} introduce chemical specificity to our calculation model. It is the binding constants that allow us to distinguish between ionic groups that are electrostatically indistinguishable. The availability of reliable K_{int} data is unfortunately limited for many systems, and reported values can vary over several orders of magnitude. Tocanne and Teissié[29] have critically analyzed and tabulated intrinsic binding constants and pK_a's for a number of phospholipids and metal ions in different geometries. When corrected K_{int}'s are unavailable, binding constants derived for water soluble molecules have been shown to be useful approximations.[28] We limit the uncertainties introduced by K_{int} values in our analysis by considering relatively well-characterized monolayer headgroups: carboxylic acid and phosphatidylserine. The intrinsic binding constants used in this work are provided in Table 1. An important aspect of future work in surface-directed mineralization will be the determination of improved intrinsic binding constants for a range of ions and headgroup functionalities and geometries.

Our calculations treat the binding of H^+, monovalent cations N^+, and divalent cations M^{2+} at the charged surface. The mass action expressions (eq 4) can be written: $\{HL^0\} = K_{HL}\{L^-\}[H^+]_0$, $\{NL^0\} = K_{NL}\{L^-\}[N^+]_0$, and $\{ML^+\} = K_{ML}\{L^-\}[M^{2+}]_0$.

An expression for the surface charge density (σ) after ion binding is developed by algebraic manipulation of charge and site balances:[36]

$$\sigma = \frac{-e\{L\}^{tot}[1 - K_{ML}[M^{2+}]_0]}{[1 + K_{HL}[H^+]_0 + K_{NL}[N^+]_0 + K_{ML}[M^{2+}]_0]} \tag{5}$$

Note that $\{L\}^{tot}$ is simply the inverse of the area per lipid molecule, $1/A_m$.

Finally, the surface charge density (σ) can be related to the surface potential ($\Psi(0)$) using the Grahame equation, which was originally derived from the PB equation using the boundary condition that the excess charge density in the electric double layer balances the surface charge:[44]

$$\sigma = -\left[2\epsilon\epsilon_0 kT \sum_i^m n_{i,b}\left[\exp\left(\frac{-z_i e\Psi(0)}{kT}\right) - 1\right]\right]^{1/2} \tag{6}$$

Equations 5 and 6 and the mass action expressions of eq 4 define a system of equations that can be solved simultaneously to determine the unknowns $\Psi(0)$, σ, $[H^+]_0$, $[N^+]_0$,$[M^{2+}]_0$. We perform this calculation using a commercial root-finding software procedure (Mathematica). The fractional ion condensation[28] Γ_i is used to describe the Stern layer of bound ions at the surface. Γ_i is the bound ion-to-lipid ratio:

$$\Gamma_i = \frac{\{ML\}}{\{L\}^{tot}} \tag{7}$$

The fractional ion condensation expressions are written: $\Gamma_H = \{HL^0\}/\{L\}^{tot}$, $\Gamma_N = \{NL^0\}/\{L\}^{tot}$, and $\Gamma_M = \{ML^+\}/\{L\}^{tot}$.

Results and Discussion

The general model described above has been used to assess the interfacial electrostatic parameters and ion distributions for various surface-directed mineralization conditions. The calculations provide a description of the interfacial environment within which heterogeneous mineral nuclei form and show how the interfacial solution chemistry varies with changes in the bulk solution. Representative calculations provide a quantitative basis on which to explore the functional relationship between electrostatics and the molecular mechanisms of oriented nucleation.

Surface Parameters and Double Layer Profiles for Different Bulk Solutions. Carboxylates such as stearic acid monolayers have been used as templates in several oriented crystallization studies.[7−9,19−20] The electrostatic properties of these systems are therefore of particular interest. Table 2 provides surface electrostatic parameters for carboxylic acid monolayers (20 Å^2 per molecule) contacting three equimolar bulk solutions at 25 °C and pH 6: $[CaCl_2] = [Na_2A] = 10.0$, 1.0, and 0.1 mM. A and A^{2-} are used throughout this section to represent anions such as $C_2O_4^{2-}$ and SO_4^{2-}. Figure 2 shows how the ion concentrations in the aqueous phase adjacent to the surface ($[Ca^{2+}]_0$ and $[A^{2-}]_0$) and the effective surface pH vary with bulk solution concentrations.

The carboxylic acid monolayer calculations show clear trends: the surface charge density (σ) is significantly neutralized by counterion binding for all three solution conditions (Table 2), the Stern surface potential ($\Psi(0)$) shows an approximately 30 mV increase with each order of magnitude decrease in the Ca^{2+} concentration in the bulk (Table 2), and the Ca^{2+}

TABLE 2: Surface and Double Layer Parameters for Carboxylic Acid Monolayers Contacting Different Bulk Solutions at pH 6[a]

surface parameter[b]	10 mM	1 mM	0.1 mM
σ (C/m$^{2)}$	−0.033	−0.030	−0.026
$\Psi(0)$ (mV)	−42.5	−70.8	−96.9
thickness, $1/e$ (Å)	11	27	65
thickness, $1/\kappa$ (Å)	12	40	125
Γ_{Ca}	0.31	0.14	0.048
Γ_{Na}	<0.01	<0.01	<0.01
Γ_H	0.41	0.69	0.87

[a] The concentrations listed in the column headings give the $[CaCl_2] = [Na_2A]$ concentration in the bulk solution. A and A^{2-} represent divalent anions such as SO_4^{2-} and $C_2O_4^{2-}$. The solutions were at pH 6 and 25 °C. Monolayer packing was 20 Å^2 per molecule. [b] σ is the surface charge density, $\Psi(0)$ is the Stern surface potential, thickness $1/e$ is the first e−folding of the electric potential decay,and$1/\kappa$ is the Debye length; the fractional ion condensations Γ_i give the bound ion to lipid ratio at the surface.

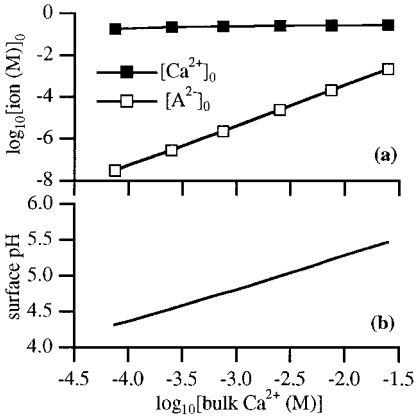

Figure 2. Interfacial parameters for a carboxylic acid monolayer (20 Å^2 per molecule) contacting equimolar ($[CaCl_2] = [Na_2A]$) bulk solutions at 25 °C and pH 6. A and A^{2-} represent inorganic divalent anions such as $C_2O_4^{2-}$ and SO_4^{2-} The horizontal axis is the logarithm of the bulk $[Ca^{2+}]$ concentration (M), equal to the bulk $[A^{2-}]$. (a) $[Ca^{2+}]_0$ and $[A^{2-}]_0$ concentrations in the aqueous phase adjacent to the surface ($x = 0$). (b) Effective surface pH.

concentration in the aqueous phase at the monolayer surface is independent of the concentration in the bulk (Figure 2a). The latter two points are manifestations of the well-established contact value theorem of Gouy−Chapman theory.[26,27] The fractional ion condensation calculations, Γ_i, provide insight into ion binding at the interface. Γ_{Ca} and Γ_H (Table 2) show that Ca^{2+} and H^+ compete for binding sites for bulk pH 6 solutions.

Multivalent co-ion distributions are not normally considered in detail in GCS analyses, because their contribution to the interfacial electric potential is small. Co-ion distributions, however, are extremely important in the context of mineralization since they are required for the formation of the nucleating mineral unit cell. Unlike the counterions, which have interfacial solution concentrations independent of the bulk, interfacial co-ion concentrations (A^{2-}) vary as the bulk solution concentration is varied, reflecting the repulsive interaction with the changing electric potential (Figure 2a). For each order of magnitude decrease in the divalent ion concentration in the bulk, a 2 orders of magnitude decrease in the divalent anion concentration at the surface is observed. Implications for mineral nucleation are addressed shortly.

Figure 3 illustrates the potential and pH profiles for our three model solutions as a function of distance away from the carboxylic acid surface. Also included in Figure 3a are the profiles predicted by the Debye−Hückel expression,$\Psi(x) = \Psi(0)$ $\exp^{-\kappa x}$. Here we see that the double-layer thickness predicted by integration of eq 3 can be significantly smaller than that predicted by the more familiar Debye−Hückel expression, a result consistent with experiment.[32] Figures 2b and 3b show that despite the constant bulk solution pH (pH 6), the effective pH is lowered near the negatively charged surface and varies for the different bulk solutions (the effective pH is defined as the negative logarithm of the H^+ concentration[43]). The degree of the pH lowering depends on the magnitude of the surface potential, which in turn is a function of both monolayer (chemistry and geometry) and bulk solution properties. Because solubility and supersaturation of many minerals vary strongly with pH, the assessment of interfacial pH is important when describing mineralization at charged surfaces.

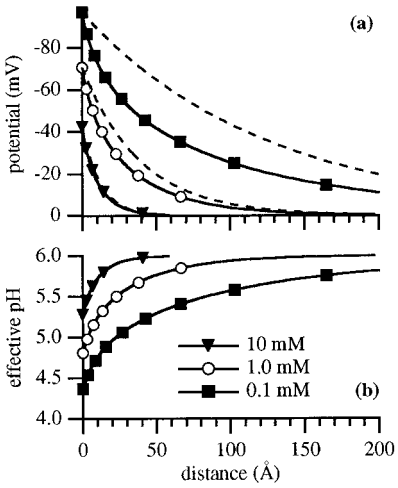

Figure 3. Potential and pH profiles as a function of distance away from a carboxylic acid monolayer (20 Å^2 per molecule) contacting aqueous solutions with bulk $[CaCl_2] = [Na_2A] = 10$, 1.0, and 0.1 mM at pH 6 and 25 °C. A and A^{2-} represent inorganic divalent anions such as CO_3^{2-} and SO_4^{2-} (a) Electric potential: the solid lines with markers were calculated by numerical integration of the Poisson−Boltzmann equation (eq 3); the dashed lines are the Debye−Hückel profiles for each solution (see text). (b) Effective pH.

Bulk solution pH is a parameter commonly used to influence surface-directed mineralization. In addition to altering mineral solubilities, pH changes in the bulk can also alter ion condensation at the monolayer surface. For example, consider the $[CaCl_2] = [Na_2A] = 1$ mM solution contacting the carboxylic acid monolayer. At pH 6, the fractional Ca^{2+} condensation Γ_{Ca} was 0.14 and Γ_H was 0.69 (Table 2). If we repeat the calculation for a bulk pH 8, Γ_{Ca} becomes 0.47 and Γ_H is 0.02. The Stern surface potential $\Psi(0)$ remains approximately −70 mV in both cases. The charge compensation lost by deprotonation at higher pH is regained by increased Ca^{2+} binding. The nature of the bound Stern layer is very different in the two bulk pH regimes.

Figure 4 shows the Ca^{2+} and A^{2-} ion distributions for the three solutions described in Table 2. Near the surface, Ca^{2+} ion profiles roughly coincide for all three bulk solutions, again a manifestation of the so-called contact value theorem.[26−27] Alternatively, the A^{2-} concentration profiles in the interface region vary strongly for the different bulk solutions. Implications of this chemical anisotropy are discussed below.

Mineral Nucleation within the Double Layer of a Charged Surface. The model calculations discussed above are representative of conditions in much of the surface-directed mineralization literature. The double-layer thicknesses calculated for these solutions ranged from approximately 10 to 100 Å. Embryonic heterogeneous mineral nuclei are believed to be comprised of a few to tens of ions and are likely less than 15

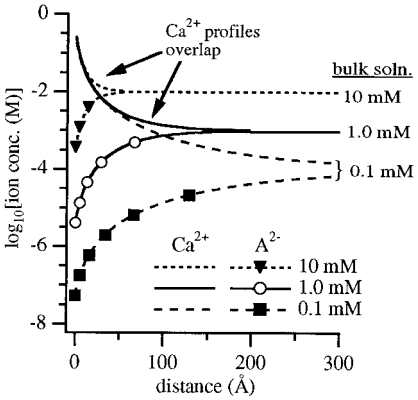

Figure 4. Semilog plot of Ca^{2+} and A^{2-} ion concentration profiles as a function of distance away from a carboxylic acid monolayer (20 Å^2 per molecule) contacting aqueous solutions with bulk $[CaCl_2] = [Na_2A] = 10$, 1.0, and 0.1 mM at pH 6 and 25 °C. A and A^{2-} represent inorganic divalent anions such as $C_2O_4^{2-}$ and SO_4^{2-}. The Na^+ and Cl^- profiles are not shown.

Å in diameter. If three-dimensional nuclei are initiated at the surface (heterogeneous nucleation), then they form within the physically and chemically anisotropic double-layer environment. Classical nucleation theory was developed by analogy with liquid condensation from the vapor phase. Wu and Nancollas[21] have recently shown that nucleation in aqueous solution cannot be fully explained by the classical theory because electric double-layer effects are not accounted for in the free energy expressions. In addition to these important thermodynamic arguments, chemical anisotropies near charged surfaces raise further complications.

The cation concentration enhancement observed at negatively charged surfaces has been assumed to imply increased mineral supersaturation.[4,16] It is not clear, however, that such a correlation is easily established. Near a negatively charged surface, cation concentration enhancement and anion repulsion lead to departures from lattice ion stoichiometry. Studies of inorganic crystallization in bulk solutions have shown that the thermodynamic driving force (supersaturation) does not fully describe observations when the electrolyte solution is nonstoichiometric with respect to the crystal lattice unit cell.[45−47] Nucleation rates, growth rates, crystal solubilities and phase are all functions of the cation-to-anion ratio.[45−47] By analogy with these bulk solution studies, we propose that similar effects could occur in the local solution near a charged surface when departures from stoichiometry are large. In addition, the lower effective pH near negatively charged surfaces could also alter supersaturation by increasing mineral phase solubility. The pH dependence of supersaturation is significant for many minerals, including the biologically relevant calcium phosphates and calcium carbonates. We believe these arguments are consistent with experimental observations and note that not all negatively charged surfaces are good nucleators. One would expect enhanced nucleation at more negative surfaces if cation concentration enhancement simply increased supersaturation. For example, Addadi et al.[4] showed that polystyrene films sulfonated for 8 h were much more effective at promoting oriented calcite nucleation than films sulfonated for 24 h, despite the fact that the latter had twice as many sulfonate groups. Similarly, Campbell et al.[14] noted that calcium oxalate monohydrate nucleation was less effective on highly charged thiazoladine self-assembled monolayers than on neutral imidazole monolayers. Charge compensation by ion binding is limited in the thiazoladine case because carboxylate groups are oriented away from the solution.[14] Numerous factors certainly contribute to nucleation rates and number densities. Nevertheless, the departure from lattice ion stoichiometry and the lower pH near highly charged surfaces could be contributing factors. In addition to any templating effects, a functional role of specific cation binding to nucleating matrices in biomineralization therefore may be to limit the repulsion of co-ions from the surface. This lattice ion stoichiometry argument is conceptually similar to the interfacial kinetics arguments presented by Stumm and coworkers.[48] Those authors showed that despite a close epitaxial match, CaF_2 overgrowth on CeO_2 substrates was only effective in a pH range where both lattice ions (Ca^{2+} and F^-) adsorbed to the surface.[48]

Molecular Recognition and Lattice Matching. The term "molecular recognition" is frequently used when describing surface- or template-directed crystallization. In general, molecular recognition can be said to include all interactions exhibiting chemical specificity. As noted earlier, cation binding to the monolayer is not merely an electrostatic effect and chemical specificity exists. Carboxylates and sulfonates, for example, differ in their ability to bind Ca^{2+}.[4] Not only does this affect the nature of a bound cation array in the plane of the surface, it also affects the magnitude of interfacial physical and chemical anisotropies (e.g., cation-to-anion ratio, pH, etc.) as discussed above. In this respect, molecular recognition, electrostatics, and interfacial chemistry are linked. Organisms may exploit this molecular recognition between organic surfaces and ions to effectively "tune" interfacial solution chemistry, influencing subsequent mineralization events.

Lattice matching or epitaxy between an organic template and inorganic crystals has received considerable attention in the literature. The data provided in this paper allow a more quantitative interpretation of this effect. A component of the lattice matching argument has been the formation of an ordered array of bound cations that mimics a particular plane in a nucleating inorganic crystal surface.[8,9] For example, the interheadgroup spacing of a compressed stearate monolayer (∼5 Å) provides a close epitaxial match with $Ca^{2+}-Ca^{2+}$ distances in Ca^{2+}-rich calcite planes (4.96 Å).[8] Presumably, a bound Ca^{2+} Stern layer at such a monolayer preferentially nucleates calcite through a geometric match. This argument has been invoked to explain the vaterite to calcite phase switch at carboxylate monolayers as the Ca^{2+} concentration in the supersaturated subphase is increased.[8,9] Those authors argue that at lower Ca^{2+} concentrations (<4.5 mM), the lack of a Stern layer leads to vaterite nucleation, while the well-defined Stern layer at higher concentrations (9 mM) catalyzes calcite nucleation. Calculations using the methodology described in our paper, however, do not support this argument. The Stern layer (given by Γ_{Ca}) is quite similar for 4.5 and 9 mM Ca^{2+} solutions: $\Gamma_{Ca} = 0.22$ and 0.26, respectively. Furthermore, Γ_{Ca} is ≤ 0.5 for all experimental conditions we have investigated. $Ca^{2+}-Ca^{2+}$ separations in the bound Stern layer are therefore larger than the headgroup spacings. The cation-to-anion ratio near the carboxylic acid monolayer may be a more important factor in the vaterite−calcite example. The departure from lattice ion stoichiometry is significantly larger for low Ca^{2+} concentration solutions (as shown in Figure 2a), which may favor vaterite because of its more disordered structure.[49]

Ion Speciation and Orientation. The repulsion of multivalent anions from negatively charged surfaces raises the issue of how anions are delivered to the surface for nucleation. In this section we propose a link between anion speciation and oriented nucleation at charged surfaces. This discussion is especially relevant in light of recent X-ray reflectivity measurements[18] suggesting that instead of free ions, the "counterions"

TABLE 3: Electrostatic Parameters and Bulk Solution Speciation[50] for the Phosphatidylserine−Calcium Oxalate System[a]

surface parameter		species	concn (μM)
σ (C/m$^{2)}$	−0.021	Ca^{2+}	180
$\Psi(0)$ (mV)	−62.8	$C_2O_4^{2-}$	170
thickness, *1/e* (Å)	25	$[Ca(C_2O_4)]^0$	36
thickness, *1/κ* (Å)	29	$[Na(C_2O_4)]^-$	15
Γ_{Ca}	0.44	$[H(C_2O_4)]^-$	0.78
Γ_{Na}	0.036	$[Ca_2(C_2O_4)]^{2+}$	0.47
Γ_H	0.018	$[Ca(C_2O_4)_2]^{2-}$	0.10
		$[Ca(OH)]^+$	

[a] The bulk solution contained 0.22 mM $CaCl_2$, 0.22 mM $Na_2C_2O_4$ and 10 mM NaCl at pH 6 and 25 °C. Phosphatidylserine (PS) occupied 46 Å^2 per molecule in the monolayer.

near negatively charged surfaces, especially at high pH (>6), are complex species such as $[CdOH]^+$.

We address ion speciation in relation to surface-directed mineralization using calcium oxalate (CaC_2O_4) nucleation at phospholipid monolayers as a model system. Our experimental conditions have been described elsewhere.[20] Briefly, the bulk solution contains total $[CaCl_2] = [Na_2C_2O_4] = 0.22$ mM and 10 mM [NaCl] at 25 °C and pH 6. The surface is a phosphatidylserine (DMPS) monolayer compressed to 46 Å^2 per molecule. Table 3 provides the electrostatic surface parameters for this system as well as the bulk solution speciation.[50] Although the species concentrations are all lower than the free ion concentrations, their net charges are important to consider in relation to a negatively charged surface. For example, unlike C_2O_4,$^{2-}$ the neutral complex $[Ca(C_2O_4)]^0$ experiences no electrostatic repulsion, and $[Ca_2(C_2O_4)]^{2+}$ is electrically attracted to the surface.

Unfortunately, a quantitative assessment of speciation in the double layer will require an electrochemical equilibrium model beyond the scope of the current analysis. We can, however, anticipate trends by introducing alternate simplifying assumptions. First, Figure 5a shows the calculated ion distributions if we assume the species remain in tact across the electric double layer. These purely electrostatic calculations suggest that the $[Ca(C_2O_4)]^0$ and $[Ca_2(C_2O_4)]^{2+}$ concentrations near the surface may be higher than that of the free $C_2O_4^{2-}$ ion. Since these species are comprised of mineral lattice ions, it is reasonable to assume they will participate in nucleation. The Figure 5a results, however, fail to address the fact that the relative concentrations of the equilibrium species will be altered within the nonstoichiometric solution environment of the double layer. Alternatively, our second simplifying assumption approximates this altered equilibrium by estimating speciation for nonstoichiometric bulk solutions, as in Figure 5b. The calculations provide insight into the chemical contributions to the electrochemical equilibrium. The left side of the plot shows speciation for a Ca^{2+}-rich solution, intended to simulate chemical conditions near a negatively charged surface. The $C_2O_4^{2-}$-rich solution on the right simulates conditions near a positively charged surface. We note that the Ca^{2+}-rich environment favors formation of the $[Ca(C_2O_4)]^0$ and $[Ca_2(C_2O_4)]^{2+}$ species at the expense of free $C_2O_4^{2-}$. Thus, both approximations in Figure 5 suggest that the relative concentrations of the soluble calcium oxalate species will be enhanced near negatively charged surfaces. The point here is that in addition to free anions, molecular species possibly play a role in oriented mineral nucleation at negatively charged surfaces. Future molecular models of nucleation at charged surfaces will require both theoretical and experimental assessment of complex ions in the interface region.

We close with a comment on orientation of molecular species and nuclei. Species such as $[Ca(C_2O_4)]^0$ have a permanent

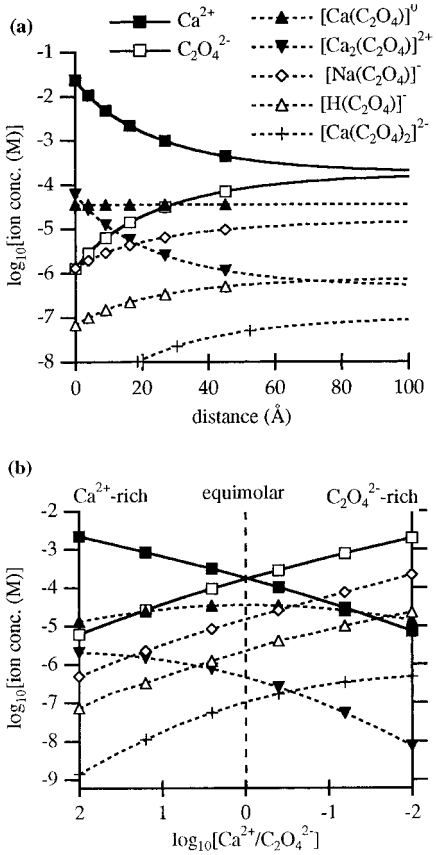

Figure 5. (a) Semilog plot of ion concentrations as a function of distance away from a phosphatidylserine monolayer (46 Å^2 per molecule) contacting a speciated calcium oxalate solution with total $[CaCl_2] = [Na_2C_2O_4] = 0.22$ and 10 mM NaCl at 25 °C and pH 6 (see Table 3). The ion profiles were calculated by assuming that the molecular species remain intact across the double layer. (b) Calcium oxalate speciation in nonstoichiometric bulk solutions. The horizontal axis is the logarithm of the total Ca^{2+} to total $C_2O_4^{2-}$ ratio in the solution. The dashed equimolar line corresponds to the bulk solution described in (a). The Ca^{2+}-rich left axis corresponds to a bulk solution with total $[CaCl_2] = 2.2$ mM and $[Na_2C_2O_4] = 0.022$ mM and is intended to simulate the chemical environment near a negatively charged surface. The $C_2O_4^{2-}$-rich right axis represents a $[CaCl_2] = 0.022$ mM and $[Na_2C_2O_4] = 2.2$ mM solution and correspond to a positive surface. All solutions contained 10 mM NaCl and were at 25 °C and pH 6.

dipole moment and therefore can be expected to orient in an interfacial electric field. We believe this orientation mechanism may contribute to our observation of two distinct $CaC_2O_4-H_2O$ morphologies beneath neutral and negatively charged lipid monolayers.[20] In situ optical microscope images of the two morphologies, as viewed through the lipid monolayer, are provided in Figure 6. Figure 6a shows the common prismatic $CaC_2O_4-H_2O$ morphology, with the broad $(\bar{1}01)$ face oriented parallel to the monolayer. Planar $C_2O_4^{2-}$ ions lie within the $(\bar{1}01)$ face and are therefore also oriented parallel to the monolayer. This morphology is consistently observed beneath neutral or zwitterionic monolayers.[20] Figure 6b shows the general crystal morphology observed beneath negatively charged monolayers. These crystals contact the monolayer at a point rather than on a broad face and do not show the well-developed $(\bar{1}01)$ crystal planes parallel to the monolayer. The observed morphology differences cannot be fully explained by lattice geometry or traditional stereochemical arguments.[20] We postulate that the perpendicular alignment of $[Ca(C_2O_4)]^0$ species near the negatively charge lipid surfaces could inhibit formation of the $(\bar{1}01)$ face parallel to the monolayer, resulting in the observed morphology.

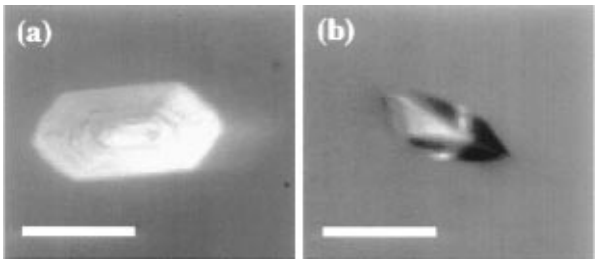

Figure 6. In situ optical microscope images of $CaC_2O_4-H_2O$ crystals grown at lipid monolayers in a Langmuir trough;[20] the crystals are imaged through the lipid monolayer from above using the brightfield mode of an epi-fluorescence microscope. (a) The prismatic crystal morphology grown beneath zwitterionic dipalmitoylphosphatidylcholine (DPPC) monolayers. (b) The crystal morphology grown beneath negatively charged dimyristoylphosphatidylserine (DMPS) monolayers. Scale bar = 10 μm.

Conclusions

Mineralization at charged surfaces is dictated by poorly understood interfacial phenomena, and no single factor dominates oriented nucleation. In this paper a quantitative assessment of surface electrostatic parameters and interfacial ion distributions provided the basis for an investigation of electrostatic contributions to oriented nucleation. The intent of this work was to augment existing interpretations of oriented mineral nucleation that have relied on qualitative electrostatic arguments. In addition to quantifying commonly discussed phenomena such as the formation of a bound cation layer, the calculations presented here suggested that subtle bulk solution changes can significantly alter the interfacial chemical environment within which nuclei form. In particular, the departure from mineral lattice ion stoichiometry and interfacial pH lowering near negatively charged nucleating surfaces may contribute to observed variations in mineral phase, density, and morphology. Anion speciation was shown to be potentially significant near negatively charged surfaces, and a link between ion speciation and oriented mineral nucleation at charged surfaces was proposed. Experiments are currently underway in our laboratory to further elucidate electrostatic effects.

Acknowledgment. The authors gratefully acknowledge mineralization discussions with Drs. Allison Campbell, Peter Rieke, and Barbara Tarasevich. Financial support was provided by the Battelle Pacific Northwest National Laboratory, Task 234509-AF2, and by the University of Washington Engineered Biomaterials NSF Engineering Research Center.

References and Notes

(1) Lowenstam, H. A.; Weiner, S. *On Biomineralization*; Oxford: New York, 1989.
(2) Addadi, L.; Weiner, S. *Angew. Chem., Int. Ed. Engl.* **1992**, *31*, 153.
(3) Addadi, L.; Weiner, S. *Proc. Natl. Acad. Sci. U.S.A.* **1985**, *82*, 4110.
(4) Addadi, L.; Moradian, J.; Shay, E.; Maroudas, N. G.; Weiner, S. *Proc. Natl. Acad. Sci. U.S.A.* **1987**, *84*, 2732.
(5) Belcher, A. M.; Wu, X. H.; Christensen, R. J.; Hansma, P. K.; Stucky, G. D.; Morse, D. E. *Nature* **1996**, *381*, 65.
(6) Landau, E. M.; Levanon, M.; Leiserowitz, L.; Lahav, M.; Sagiv, J. *Nature* **1985**, *318*, 353.
(7) Mann, S.; Archibald, D. D.; Didymus, J. M.; Douglas, T.; Heywood, B. R.; Meldrum, F. C.; Reeves, N. J. *Science* **1993**, *261*, 1286.
(8) Mann, S.; Heywood, B. R.; Rajam, S.; Walker, J. B. A. *J. Phys. D: Appl. Phys.* **1991**, *24*, 154.
(9) Heywood, B. R.; Mann, S. *Adv. Mater.* **1994**, *6*, 9.
(10) Bunker, B. C.; Rieke, P. C.; Tarasevich, B. J.; Campbell, A. A.; Fryxell, G. E.; Graff, G. L.; Song, L.; Liu, J.; Virden, J. W.; McVay, G. L. *Science* **1994**, *264*, 48.
(11) Calvert, P.; Rieke, P. *Chem. Mater.* **1996**, *8*, 1715.
(12) Fendler, J. H. *Chem. Mater.* **1996**, *8*, 1616.
(13) Feng, S.; Bein, T. *Nature* **1994**, *368*, 834.
(14) Campbell, A. A.; Fryxell, G. E.; Graff, G. L.; Rieke, P. C.; Tarasevich, B. J. *Scanning Microsc.* **1993**, *7*, 423.
(15) Rieke, P. C.; Wiecek, R.; Marsh, B. D.; Wood, L. L.; Liu, J.; Song, L.; Fryxell, G. E.; Tarasevich, B. J. *Langmuir* **1996**, *12*, 4266. Rieke, P. C.; Marsh, B. D.; Wood, L. L.; Tarasevich, B. J.; Liu, J.; Song, L. Fryxell, G. E. *Langmuir* **1995**, *11*, 318.
(16) Archibald, D. D.; Qadri, S. B.; Gaber, B. P. *Langmuir* **1996**, *12*, 538.
(17) Berman, A.; Ahn, D. J.; Lio, A.; Salmeron, M.; Reichert, A.; Charych, D.; *Science* **1995**, *269*, 515.
(18) Li, J.; Liang, K. S.; Scoles, G.; Ulman, A. *Langmuir* **1995**, *11*, 4418.
(19) Ma, C. L.; Lu, H. B.; Wang, R. Z.; Zhou, L. F.; Cui, F. Z.; Qian, F. *J. Cryst. Growth* **1997**, *173*, 141.
(20) Letellier, S. R.; Lochhead, M. J.; Campbell, A. A.; Vogel, V. *Biochim. Biophys. Acta*, in press.
(21) Wu, W.; Nancollas, G. H. *J. Colloid Interface Sci.* **1996**, *182*, 365.
(22) Jacquemain, D.; Grayer Wolf, S.; Leveiller, F.; Deutsch, M.; Kjaer, K.; Als-Nielsen, J.; Lahav, M.; Leiserowitz, L. *Angew. Chem., Int. Ed. Engl.* **1992**, *31*, 130.
(23) Verwey, E. J. W.; Overbeek, J. Th. G. *Theory of the Stability of Lyophobic Colloids*; Elsevier: New York, 1948.
(24) Davies, J. T.; Rideal, E. K. *Interfacial Phenomena*; Academic Press: New York, 1961.
(25) Adamson, A. W. *Physical Chemistry of Surfaces*; John Wiley and Sons: New York, 1990.
(26) Israelachvili, J. *Intermolecular and Surface Forces*; Academic Press: New York, 1992.
(27) McLaughlin, S. *Annu. Rev. Biophys. Biophys. Chem.* **1989**, *18*, 113.
(28) Bloch, J. M.; Yun, W. *Phys. Rev. A* **1990**, *41*, 844.
(29) Tocanne, J. F.; Teissié, J. *Biochim. Biophys. Acta* **1990**, *111*, 1031.
(30) Peitzsch, R. M.; Eisenberg, M.; Sharp, K. A.; McLaughlin, S. *Biophys. J.* **1995**, *68*, 729.
(31) Bloch, J. M.; Yun, W. B.; Yang, X.; Ramanathan, M.; Montanamo, P. A.; Capasso, C. *Phys. Rev. Lett.* **1988**, *61*, 2941.
(32) Bedzyk, M. J.; Bommarito, G. M.; Caffrey, M.; Penner, T. L. *Science* **1990**, *248*, 52.
(33) Calvert, P.; Mann, S. *Nature* **1997**, *386*, 127.
(34) Du, Q.; Freysz, E.; Shen, Y. R. *Phys Rev. Lett.* **1994**, *72*, 238.
(35) Torrie, G. M.; Valleau, J. P.; Patey, G. N. *J. Chem. Phys.* **1982**, *76*, 4615.
(36) McLaughlin, S.; Mulrine, N.; Gresalfi, T.; Vaio, G.; McLaughlin, A. *J. Gen. Physiol.* **1981**, *77*, 445.
(37) Nir, S.; Newton, C.; Papahadjopoulos, D. *Bioelectrochem. Bioenerg.* **1978**, *5* 116.
(38) Lösche, M.; Helm, C.; Mattes, H. D.; Möhwald, H. *Thin Solid Films* **1985**, *133*, 51.
(39) Pezron, E.; Claesson, P. M.; Berg, J. M.; Vollhardt, D. *J. Colloid Interface Sci.* **1990**, *138*, 245.
(40) Ahn, D. J.; Franses, E. I. *AIChE J.* **1994**, *40*, 1046.
(41) Martell, A. E.; Smith, R. M. *Critical Stability Constants* Plenum: New York, 1972.
(42) Yazdanian, M.; Yu, H.; Zografi, G. *Langmuir* **1990**, *6*, 1093.
(43) Betts, J. J.; Pethica, B. A.; *Trans. Faraday Soc.* **1956**, *52*, 1581.
(44) Grahame, D. C. *Chem. Rev. (Washington, D.C.)* **1947**, *41*, 441.
(45) Zhang, J.; Nancollas, G. H. *J. Cryst. Growth* **1992**, *118*, 287.
(46) Liu, Y.; Nancollas, G. H. *J. Cryst. Growth* **1996**, *165*, 116.
(47) Keller, D. M.; Messing, R. E.; Hileman, Jr., O. E. *Can. J. Chem.* **1980**, *58*, 2127.
(48) Stumm, W. *Chemistry of the Solid-Water Interface*; John Wiley and Sons: New York, 1992; p 226.
(49) Turnbull, A. G. *Geochim. Cosmochim. Acta* **1973**, *37*, 1593.
(50) Ion speciation was approximated using literature association constants and an iterative computer procedure. Mean activity coefficients were calculated using the Davies equation (ref 24). The values reported are for bulk solutions; no surface effects are considered.